Theoretical investigation of barium-helium collisions. II. The excitation transfer cross sections

J. Brust
Institut für Physik, Universität Hohenheim, Garbenstrasse 30, 70599 Stuttgart, Germany

Chris H. Greene
Department of Physics and JILA, University of Colorado, Boulder, Colorado 80309-0440

(Received 20 December 1996)

We develop a theoretical description of collisions between an excited barium atom in the $6s6p\ ^3P_J$, $6s5d\ ^1D_2$, or $6s5d\ ^3D_J$ state and a helium atom in the ground state. Using the adiabatic potential curves presented in the preceding paper, state-to-state cross sections are obtained from a fully quantum-mechanical close-coupling calculation using the generalized log-derivative approach. Our theoretical results are compared to recent experimental data. [S1050-2947(97)09709-6]

PACS number(s): 34.20.−b, 34.50.Pi

I. INTRODUCTION

Collisions between excited alkaline-earth metals and ground-state noble-gas atoms (NG) have generated extensive experimental and theoretical interest, since they constitute relatively simple test cases for atomic collision processes that include electronic excitations. Theoretical investigations have largely been restricted to the lighter alkaline-earth metals Mg [1–3] and Ca [1,4–6], although many interesting experimental results have been obtained for Sr-NG and Ba-NG collisions [7–15].

The first calculation of Ba-NG potential curves was performed by Czuchaj *et al.* [16,17] in order to explain the quasistatic line profile [18] and collisional redistribution of the Ba resonance line in the presence of noble-gas perturbers. The authors focused on the interaction of Ba atoms excited to the $6s6p\ ^1P_1$ state; for this reason they omitted the spin-orbit interaction of an electron in the field of the Ba^{2+} core from their calculation. Inclusion of the spin-orbit interaction is crucial, however, to explain the prominent excitation transfer processes between singlet and triplet states [4–6]. In the second paper Czuchaj *et al.* [17] included the spin-orbit interaction for the $6s6p\ ^{1,3}P_J$ states and found the avoided crossing responsible for the $^1P_1$-$^3P_2$ transfer measured by Breckenridge and Merrow [9]. To date, however, these results have not been able to explain the singlet-triplet exchange collisions and the fine-structure transfer between low-lying states of the Ba atom, which have been studied in recent experiments [12–15]. These reactions are of particular interest, since many experiments use diode laser pumping of the $^3P_1$ state; in a buffer gas atmosphere this always leads to radiative and collisional quenching into the ^3D_J states. These processes can result in a very strong buildup of metastable population (up to 80%) and in a corresponding depletion of the ground state. These effects have been used to produce a strongly excited Ba vapor for studies of energy-pooling collisions [19].

Despite the need for theoretical elucidation of these processes and confirmation of the experimental results, little effort has been made to calculate collisional cross sections using the existing potential curves. In the present paper we report a calculation of the cross sections for the recently measured excitation tranfer processes among the $6s6p\ ^3P_J$, $6s5d\ ^1D_2$, and $6s5d\ ^3D_J$ states. The preceding paper [20] presents adiabatic potential curves of the Ba-He system that were calculated, with the Ba^{2+}-e spin-orbit interaction included through a model potential. Here we report a fully quantum-mechanical close-coupling calculation of the cross sections, based on the Born-Oppenheimer potential curves and coupling terms derived from Ref. [20].

II. DESCRIPTION OF THE COLLISION DYNAMICS

In this section we develop the expressions used to calculate the cross sections. The derivation follows one of Mies [21] adapted to the present case of an excited two-electron atom that interacts with a noble-gas atom in its ground state. The collisional system is described by the Schrödinger equation

$$\left(-\frac{1}{2\mu}\frac{\partial^2}{\partial R^2}-\frac{1}{\mu R}\frac{\partial}{\partial R}+\frac{\hat{L}^2}{2\mu R^2}+\hat{H}_{BO}(\vec{R},\vec{r})\right)\Psi(\vec{R},\vec{r}) = E\Psi(\vec{R},\vec{r}), \tag{1}$$

where R is the interatomic distance, $\hat{L}$ is the relative angular-momentum operator of the atoms, μ is the reduced mass, and E is the total energy of the collision complex. $\hat{H}_{BO}$ is the the electronic Hamiltonian operator which depends on the interatomic distance R parametrically. Equation (1) must be solved subject to scattering boundary conditions in the laboratory frame,

$$\Psi(\vec{R},\vec{r})\rightarrow\exp(i\vec{k}_J\cdot\vec{R})\langle\vec{r}|\,\gamma,J,m_J\rangle+\sum_{\gamma',J',m_{J'}}\frac{\exp(ik_{J'}R)}{R} \times\langle\vec{r}|\,\gamma',J',m_{J'}\rangle f_{\gamma,J',m_{J'};\gamma,J,m_J}(\hat{k}_{J'},\hat{k}_J) \tag{2}$$

Here k_J is the atomic wave vector, J is the total electronic angular momentum of the Ba atom, and m_J is the corresponding magnetic quantum number. γ denotes the remaining electronic quantum numbers of the asymptotic electronic state. Primed variables denote the quantum state of the system after the collision. In practice, configuration space is

divided into an interaction volume with $R \leqslant R_0$ and an asymptotic region with $R > R_0$. For the purposes of the discussion below, the wave functions in the asymptotic region will be denoted by barred symbols.

The electronic wave functions, which asymptotically correlate with two-electron eigenfunctions for the barium atom, have been calculated in a body-fixed coordinate system with the z axis oriented along the interatomic axis. It is thus advantageous to express the space-fixed wave functions $\langle \vec{r} | \gamma, J, m_J \rangle$ in terms of these body-fixed wave functions $\langle \mathbf{r} | \gamma J \Omega \rangle$. Furthermore, it is convenient to make use of the conservation of the total angular momentum $\vec{N} = \vec{L} + \vec{J}$ and the total energy E by expanding $\overline{\Psi}$ in terms of eigenfunctions of N, M, and E,

$$\overline{\Psi}^{N,M,E}_{\gamma,L,J}(\vec{R},\vec{r}) = \sum_{N,M} \overline{\mathcal{F}}^{N,M,E}_{\gamma',L',J';\gamma,L,J}(R) \overline{\Psi}_{\gamma LJ}(\hat{R},\vec{r}), \quad (3)$$

where $\overline{\Psi}_{\gamma LJ}$ is the coupled wave function

$$\overline{\Psi}_{\gamma LJ}(\hat{R},\vec{r}) = (-1)^{L+J}(2L+1)^{1/2} \sum_{\Omega} (-1)^{\Omega} \times \begin{pmatrix} L & J & N \\ 0 & \Omega & -\Omega \end{pmatrix} \Omega^{N*}_{M\Omega}(\phi_R, \theta_R) \langle \vec{r} | \gamma J \Omega \rangle, \quad (4)$$

with $\Omega^{N*}_{M\Omega}(\phi,\theta)$ the normalized wave function of a symmetric top

$$\Omega^{N*}_{M\Omega}(\phi,\theta) = \left(\frac{2N+1}{4\pi} \right)^{1/2} D^{N*}_{M\Omega}(\phi,\theta,0). \quad (5)$$

An analogous expansion can be used for the molecular wave function $\Psi^{N,M,E}_{\gamma,L,J}$ within the interaction volume where the atomic basis states are mixed by the interatomic interaction. In this case the atomic wave function $\langle \vec{r} | \gamma J \Omega \rangle$ has to be replaced by the R-dependent Born-Oppenheimer wave function $\langle \vec{r} | R; \gamma J \Omega \rangle$. Within the interaction volume the radial wave function is denoted by $\mathcal{F}^{N,M,E}_{\gamma',L',J';\gamma,L,J}(R)$.

An expression for the state-to-state inelastic scattering cross section can be obtained expanding $\overline{\mathcal{F}}^{NME}_{\gamma' L' J';\gamma LJ}$ in terms of spherical Bessel and Hankel functions $j_l, h^{(2)}_l$ using the T-matrix representation

$$\overline{\mathcal{F}}^{NME}_{\gamma' L' J';\gamma LJ}(R) = j_L(k_J R)\delta_{\gamma\gamma'}\delta_{LL'}\delta_{JJ'} - T^N_{\gamma',L',J';\gamma,L,J} h^{(2)}_{L'}(k_{J'}R). \quad (6)$$

One finds for the collision amplitude [21,22]

$$f_{\gamma',J',m_{J'};\gamma,J,m_J}(\hat{k}_J,\hat{k}_{J'}) = \frac{2\pi i}{k_J} \sum_{LL'M} Y^*_{LM-m_J}(\hat{k}_J) Y_{L'M-m_{J'}}(\hat{k}_{J'}) \sum_N (-1)^{L'-J'+M}(-1)^{L-J+M}(2N+1) \times \begin{pmatrix} L' & J' & N \\ M-m_{J'} & m_{J'} & M \end{pmatrix} \begin{pmatrix} L & J & N \\ M-m_J & m_J & M \end{pmatrix} T^N_{\gamma',L',J';\gamma,L,J}, \quad (7)$$

where $T^N_{\gamma',L',J';\gamma,L,J}$ is the transition matrix in the coupled representation.

Integration over all scattering angles and averaging over all directions of the incident wave vectors yields the cross section for the process $\gamma J \rightarrow \gamma' J'$ as [21]

$$\sigma_{\gamma J,\gamma' J'} = \frac{\pi}{k_J^2} \sum_N \mathcal{P}^N_{\gamma J,\gamma' J'}, \quad (8)$$

where the partial weighted opacity $\mathcal{P}^N_{\gamma J,\gamma' J'}$ is given by

$$\mathcal{P}^N_{\gamma J,\gamma' J'} = \frac{2N+1}{2J+1} \sum_{LL'} |T^N_{\gamma' L' J',\gamma LJ}|^2. \quad (9)$$

$T^N_{\gamma',L',J';\gamma,L,J}$ is determined by matching $\mathcal{F}^{NME}_{\gamma',L',J';\gamma,L,J}(R)$ to the asymptotic radial wave functions $\overline{\mathcal{F}}^{NME}_{\gamma',L',J';\gamma,L,J}(R)$ at $R = R_0$. $\mathcal{F}^{NME}_{\gamma',L',J';\gamma,L,J}(R)$ is determined numerically inside the interaction volume by solving the close-coupling equations; these are derived by inserting Eq. (3) into the Schrödinger equation (1)

$$\sum_{L'J'} \langle R; \gamma' L' J' | \hat{\mathcal{H}} - E | R; \gamma LJ \rangle \mathcal{F}^{N,M,E}_{\gamma' L',J';\gamma L,J}(R) = 0, \quad (10)$$

with

$$\langle R; \gamma' L' J' | \hat{\mathcal{H}} - E | R; \gamma LJ \rangle = \int d^3\vec{r}_1 d^3\vec{r}_2 d\hat{\Omega}_R \Psi^*_{\gamma,L,J}(\hat{R},\vec{r}) \times (\hat{\mathcal{H}} - E) \Psi_{\gamma',L',J'}(\hat{R},\vec{r}). \quad (11)$$

Here $\hat{\mathcal{H}}$ is the Hamiltonian from Eq. (1). Expansion of these matrix elements leads to the following set of equations for the $\mathcal{F}^{N,M,E}_{\gamma',L',J';\gamma,L,J}$:

$$\sum_{LJ}\left(\frac{\partial^2}{\partial R^2}+2\mathcal{P}_{\gamma',L',J';\gamma,L,J}\frac{\partial}{\partial R}+\mathcal{Q}_{\gamma',L',J';\gamma,L,J}-\frac{\mathcal{C}_{\gamma',L',J';\gamma,L,J}}{\mathcal{R}^2}\right)\mathcal{F}^{N,M,E}_{\gamma',L',J';\gamma,L,J}(\mathcal{R})+2\mu(E-\mathcal{E}_{\gamma',L',J';\gamma,L,J})\mathcal{F}^{N,M,E}_{\gamma',L',J';\gamma,L,J}(R)=0. \tag{12}$$

The coupling matrices $\underline{\mathcal{P}}$, $\underline{\mathcal{Q}}$, $\underline{\mathcal{C}}$, and $\underline{\mathcal{E}}$ have the following matrix elements:

$$\begin{aligned}\mathcal{P}_{\gamma',L',J';\gamma,L,J}&=\left\langle R;\gamma'L'J'\left|\frac{\partial}{\partial R}\right|R;\gamma LJ\right\rangle,\\ \mathcal{Q}_{\gamma',L',J';\gamma,L,J}&=\left\langle R;\gamma'L'J'\left|\frac{\partial^2}{\partial R^2}\right|R;\gamma LJ\right\rangle,\\ \mathcal{C}_{\gamma',L',J';\gamma,L,J}&=\langle R;\gamma'L'J'|\hat{L}_R^2|R;\gamma LJ\rangle,\\ \mathcal{E}_{\gamma',L',J';\gamma,L,J}&=\langle R;\gamma'L'J'|H_{BO}|R;\gamma LJ\rangle.\end{aligned} \tag{13}$$

In most of the earlier applications of the close-coupling approach with diabatic basis sets to calculate atomic collision cross sections, the matrices $\underline{\mathcal{P}}$ and $\underline{\mathcal{Q}}$ could be assumed to be negligible [21,4]. The coupling between the diabatic basis states was introduced through the addition of an interaction operator, e.g., the spin-orbit operator, to the Hamiltonian of the system *after* the diabatic potential curves and eigenstates had been calculated. Since in our approach the spin-orbit coupling is directly included in the e^--Ba^{2+} model potential the basis set becomes inherently adiabatic and the first and second derivative couplings cannot be neglected. This causes a significant complication of the numerical treatment of the close-coupling equations that will be discussed below. First, however, we develop explicit expressions for some of the matrix elements in Eq. (13).

III. CALCULATION OF THE COUPLING MATRICES

Insertion of expression (4) into Eq. (11) and evaluation of the angular integral gives the following form for the matrix elements $\mathcal{P}_{\gamma',L',J';\gamma,L,J}$:

$$\sum_{\Omega}\begin{pmatrix}L' & J' & N'\\ 0 & \Omega & -\Omega\end{pmatrix}\begin{pmatrix}L & J & N\\ 0 & \Omega & -\Omega\end{pmatrix}\times\left\langle R;\gamma'J'\Omega\left|\frac{\partial}{\partial R}\right|R;\gamma J\Omega\right\rangle \tag{14}$$

The electronic Born-Oppenheimer states $|R;\gamma J\Omega\rangle$ were calculated by using the basis set expansion described in the preceding paper:

$$|R;\gamma J\Omega\rangle=\sum_{\gamma'J'}c_{\gamma'J'\Omega;\gamma J\Omega}(R)|\gamma'J'\Omega\rangle. \tag{15}$$

This formula, in conjunction with the orthogonality of the atomic basis states $|\gamma'J'\Omega\rangle$, yields the final expression for the radial coupling matrix element:

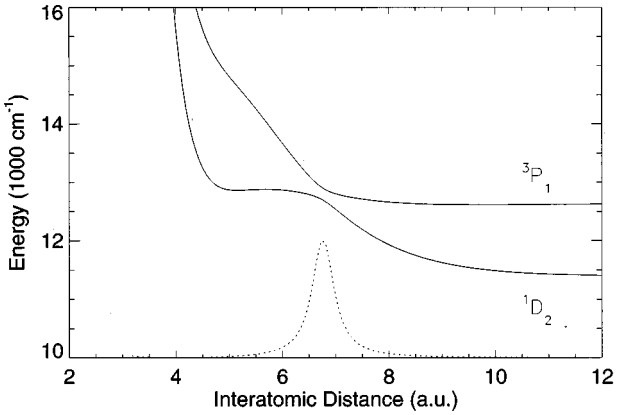

FIG. 1. Adiabatic potential curves $0(^3P_1)$ and $0(^1D_2)$ correlated to the $^3P_1$ and $^1D_2$ states. Also given is the radial coupling matrix element $\langle\gamma'J'\Omega'|\partial/\partial R|\gamma J\Omega\rangle$ ( ) in arbitrary units.

$$[(2L'+1)(2L+1)]^{1/2}\sum_{\Omega}\begin{pmatrix}L' & J' & N'\\ 0 & \Omega & -\Omega\end{pmatrix}\times\begin{pmatrix}L & J & N\\ 0 & \Omega & -\Omega\end{pmatrix}\sum_{\gamma''J''}c_{\gamma'J'\Omega;\gamma''J''\Omega}(R)\frac{\partial}{\partial R}c_{\gamma''J''\Omega;\gamma J\Omega}(R), \tag{16}$$

where the derivative operator acts on the expansion coefficients. The second derivative coupling matrix elements $\mathcal{Q}_{\gamma',L',J';\gamma,L,J}$ are given by an analogous expression.

Figures 1 and 2 show avoided crossings between the $0(^3P_1)$ and $0(^1D_2)$ and $1(^1D_2)$ and $1(^3D_3)$ potential curves, along with the radial coupling matrix element $\langle R;\gamma'J'\Omega|\partial/\partial R|R;\gamma J\Omega\rangle$ which were calculated by numerical differentiation of the expansion coefficients. The coupling matrix elements exhibit the expected Lorentzian behavior at avoided crossings; this would be consistent with the use of a Landau-Zener approximation, though we do not use that approximation here.

To calculate the coriolis coupling matrix element $\mathcal{C}_{\gamma',L',J';\gamma,L,J}$, it is advantageous to express the molecular angular-momentum operator $\vec{L}$ in terms of the conserved total ($\vec{N}$) and electronic ($\vec{J}$) angular-momentum operators,

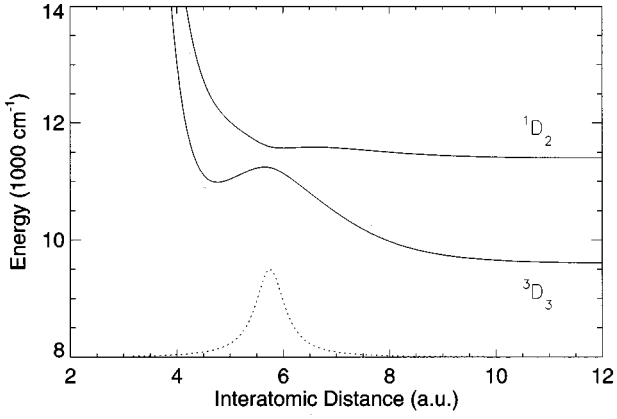

FIG. 2. Adiabatic potential curves $1(^1D_2)$ and $1(^3D_3)$ correlated to the $^1D_2$ and $^3D_3$ states. Also given is radial coupling matrix element $\langle\gamma'J'\Omega'|\partial/\partial R|\gamma J\Omega\rangle$ ( ) in arbitrary units.

$$\vec{L}=\vec{N}-\vec{J}. \tag{17}$$

Using the appropriate operator identities one finds for $\hat{L}^2$ [21,23]

$$\vec{L}^2=\hat{N}^2+\hat{J}_+\hat{J}_--\hat{N}^+\hat{J}_--\hat{N}^-\hat{J}_+-\hat{J}_z(\hat{J}_z+1). \tag{18}$$

The determination of these matrix elements proceeds along lines similar to our derivation of the radial couplings. As an example we give the explicit expression for $\langle R;\gamma' L' J'|\hat{N}^+\hat{J}_-|R;\gamma L J\rangle$:

$$\sum_{\Omega\Omega'}\begin{pmatrix} L' & J' & N' \\ 0 & \Omega' & -\Omega' \end{pmatrix}\begin{pmatrix} L & J & N \\ 0 & \Omega & -\Omega \end{pmatrix}\langle\Omega^{N*}_{M\Omega'}|\hat{N}^+|\Omega^{N*}_{M\Omega}\rangle \times\langle R;\gamma' J'\Omega'|\hat{J}_-|R;\gamma J\Omega\rangle. \tag{19}$$

Using again the expansion of the electronic wave functions in terms of the Ba states one finds for the product of matrix elements

$$\begin{aligned}\langle\Omega^{N*}_{M\Omega'}|\hat{N}^+|\Omega^{N*}_{M\Omega}\rangle\langle R;\gamma' J'\Omega'|\hat{J}_-|R;\gamma L J\rangle &= \delta_{\Omega'\Omega-1}[N(N+1)-\Omega(\Omega-1)]^{1/2} \\ &\times\sum_{\gamma'' J''} c_{\gamma' J'\Omega';\gamma'' J''\Omega'}(R)c_{\gamma'' J''\Omega;\gamma J\Omega}(R) \\ &\times[J(J+1)-\Omega(\Omega-1)]^{1/2}\end{aligned} \tag{20}$$

The superscript notation implies that $\hat{N}$ acts in the molecule-fixed space, where the commutation relations are reversed [21]:

$$N^{\pm}\Omega^N_{M\Omega}=[(N\pm\Omega)(N\mp\Omega+1)]^{1/2}\Omega^N_{M\Omega\mp1}. \tag{21}$$

IV. NUMERICAL DETAILS

Cross sections were calculated for all transfer processes involving the $6\,^3P_J$, $5\,^1D_2$, $5\,^3D_J$, and $6\,^1S_0$ states. At least one closed channel was included also, leading to systems with up to 31 coupled equations that had to be solved. Due to parity conservation in the collision process, this set of equations could be separated into two sets of half the size.

The propagation of the solution started at $R=3a_0$ with the starting condition $\mathcal{F}=0$. It was propagated out to $R_0=16a_0$. The coupling matrices were calculated on a linear radial mesh with 400 points in this region after the values for the expansion coefficients were determined by eight-point Bessel interpolation from its values on the 139-point square-root mesh used in the calculation of the potential curves [20]. During the propagation, an additional interpolation was performed in order to increase the resolution of the propagation.

A match of the resulting numerical solution at $R=R_0$ to energy-normalized spherical Bessel functions determines the reaction matrix $\underline{K}$ which in turn determines the transition matrix T^N, and finally the state-to-state cross section through Eqs. (8) and (9). The relation between the reaction and transition matrices is given by

$$\underline{T}=i\underline{K}(1+i\underline{K})^{-1}. \tag{22}$$

Since, as described above, the spin-orbit interaction was included in the Ba^{2+}-e^- interaction explicitly, the close-coupling equations contain non-negligible first-order (and second-order) derivative couplings, which makes them unsuitable for integration using standard (e.g., log-derivative [24,4]) algorithms. Therefore, we used the generalized log-derivative method [24,25], which is able to treat both the first- and second-derivative coupling terms while retaining the numerical stability characteristic of the log-derivative approach. The major drawback of this technique, however, is its numerical complexity which requires a significant number of matrix inversions during propagation. Depending on the number of equations solved, the method required up to 3 cpu-min. per angular-momentum value N. Depending on the collision energy chosen the close-coupling equations had to be solved up to a maximum value of $N=120$. Owing to the limited cpu time available, we restricted the calculations to special cases without calculating the full temperature dependence of all possible cross sections. The results of our calculations are presented in the next section.

V. RESULTS AND DISCUSSION

Figures 3 and 4 display the calculated opacity functions for the processes $6\,^3P_1$-$5\,^1D_2$ and $5\,^1D_2$-$5\,^3D_3$, plotted versus the total angular momentum. The data points are connected by lines, merely to guide the eye. The opacity function (or equivalently the partial cross section) for the process $6\,^3P_1$-$5\,^1D_2$ peaks at an angular momentum value of 33 a.u., which in the classical picture corresponds to an impact parameter of $R=4.6a_0$. At smaller values of the angular momentum the partial cross section oscillates and decreases according to the N dependence of $\mathcal{P}^{\mathcal{N}}$ in Eq. (9). At angular momenta larger than 33 the opacity function decreases as the corresponding collision parameter goes beyond the location of the avoided crossing and $6.8a_0$. The behavior of the $5\,^1D_2$-$5\,^3D_3$ is similar with the exception that at angular momenta smaller than the peak value at $23a_0$ no oscillations are observed.

From the opacity functions, the relevant cross sections were calculated from Eq. (8) by performing a sum of the partial weigthed opacities over all total angular momenta N.

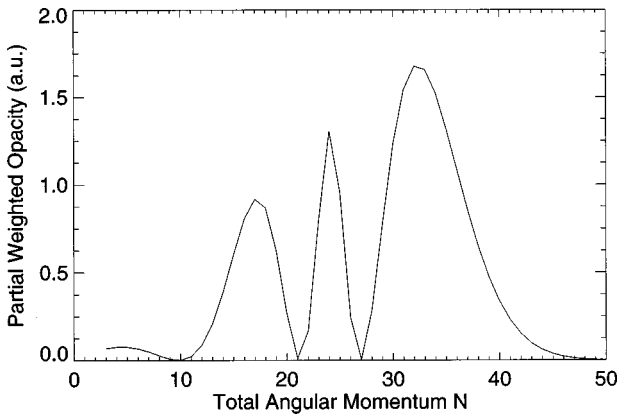

FIG. 3. Partial weighted opacity is shown versus the total-angular-momentum quantum number N, for the process $^3P_1$-$^1D_2$, at a collision energy of 610 cm^{-1}. The modulations are sometimes referred to as Stueckelberg oscillations.

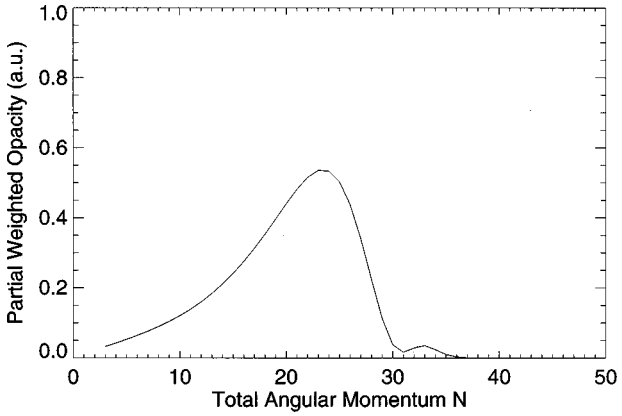

FIG. 4. Same as Fig. 3, except for the process $^1D_3$-$^3D_3$. Stueckelberg oscillations appear at energies higher than the 610 cm^{-1} collision energy at which these results were obtained.

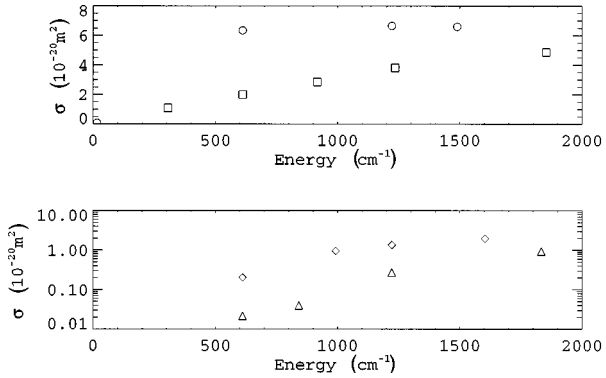

FIG. 5. Energy dependence of the cross section of the processes $^3P_1$-$^1D_2$ (top ○), 5 $^1D_2$-5 $^3D_3$ (top, □), 5 $^3D_3$-5 $^3D_2$ (bottom, △), and 5 $^3D_2$-5$^3D_1$ (bottom, ◇). An energy of 610 cm^{-1} corresponds to an experimental temperature of $T=690$ K.

Figure 5 shows the collision energy dependence of cross sections for the processes 6 $^3P_1$ and 5 $^3D_2$-5 $^3D_1$. Differing behavior is observed for the different cross sections. While the cross sections for singlet-triplet transfer show a relatively weak dependence on the collision energy, the fine-structure transfer cross sections grow strongly with increasing energy. The latter behavior is typical for fine structure transfer in the adiabatic limit [8] when the collision energy is comparable to the fine-structure splitting and the potential curves involved exhibit no avoided crossing. A closer inspection of the singlet-triplet cross sections shows that between collision energies of 500 and 1500 cm^{-1}, the cross section for the process 6 $^3P_1$-5 $^1D_2$ shows almost no energy dependence while the cross section for 5 $^1D_2$-5 $^3D_3$ transfer increases with energy. This behavior can be expected since the crossing between the 0^1D_2 and $0(^3D_3)$ potential curves is more strongly avoided than the one governing the 6 $^3P_1$-5 $^1D_2$ transfer process. The splittings at the crossing points are 360 and 200 cm^{-1}, respectively. Table I compares the calculated cross sections of the singlet-triplet transfer processes with experimental results from the literature. Good agreement is found between our results and the measured cross sections for the singlet-triplet transfer processes $^3P_1$-$^1D_2$ and $^1D_2$-$^3D_3$ reported by Vadla *et al.* [14,15]. The theoretical results fall within the experimental error bars. In view of the expected monotonic increase of the cross sections with increasing temperature, and in view of the fact that the experimental values were measured at a temperature of $T=760$ K, the agreement should be even better. Slightly worse agreement exists between our values and the data reported by Brust and Gallagher [13]. The Ref. [13] cross section for the process $^3P_1$-$^1D_2$ is about 40% smaller and their result for $^1D_2$-$^3D_3$ is about 1.5 times bigger than our calculated cross section. While there are clear discrepancies between theory and experiment, the agreement is reasonably good overall. (It should be remembered that it is not necessarily adequate to compare the cross section at a definite energy E with an experiment at a definite temperature T. Ideally, it would be better to compare the thermally averaged cross sections or rate constants directly.)

The agreement is worse for the fine-structure transfer cross sections, which are presented in Table II. In particular, the theoretical value for the process 5 $^3D_3$-5$^3D_2$ is about two orders of magnitude smaller than the datum reported by Brust and Gallagher and 20 times smaller than the result of Kallenbach and Kock [26] at a temperature of $T=1100$ K.

Good agreement exists between our value of the cross section for $^3D_2$-$^3D_1$ transfer and the cross section reported by Kallenbach and Kock. These values, however, differ by a factor of 10 from the cross section measured by Brust and Gallagher. As discussed elsewhere [12,13], the data reduction method of Kallenbach and Kock, who populated the 6 $^1P_1$ state by pulsed laser excitation and measured the time-dependent state populations of up to 13 atomic and ionic states of the Ba atom, employed a complicated rate equation model including Ba-noble gas, Ba-Ba, and Ba-electron collisions, as well as radiation trapping. Judging from their results for Ba-Ar collisions as compared to the results of Ehrlacher and Huennekens [12] and Brust and Gallagher [13] in the case of ^3D_J fine-structure transfer and the measured

TABLE I. Comparison of experimental and theoretical cross sections for singlet-triplet transfer in collisions between a helium atom and an excited barium atom. The numbers cited below are collision cross sections in units of $10^{-20}m^2$.

Process	$E=691$ cm^{-1} Present theory	$kT=612$ cm^{-1} Experiment[a]	$E=610$ cm^{-1} Present theory	$kT=528$ cm^{-1} Experiment[b]	$kT=765$ cm^{-1} Experiment[c]
$^3P_1$-$^1D_2$	6.9	3.5 ± 0.7	6.3	5.5 ± 1.5	
$^1D_2$-$^3D_3$	2.5	5.3 ± 0.7	2.0	1.5 ± 0.7	0.1 ± 0.06
$^1D_2$-$^3D_2$	0.013	$\leqslant1.1$	0.01		

[a]Reference [13], $T=880$ K.
[b]Reference [14,15], $T=760$ K.
[c]Reference [26], $T=1100$ K.

TABLE II. Comparison of experimental and theoretical fine-structure transfer cross sections in Ba-He collisions. The numbers cited below are collision cross sections in units of $10^{-20}m^2$.

Process	$E=610\ \mathrm{cm}^{-1}$ Present theory	$E=691\ \mathrm{cm}^{-1}$ Present theory	$kT=612\ \mathrm{cm}^{-1}$ Experiment[a]	$kT=765\ \mathrm{cm}^{-1}$ Experiment[b]
$^3P_2-{}^3P_1$	0.0046	0.0011	$\leqslant 0.4$	0.001 ± 0.0006
$^3P_1-{}^3P_0$	6×10^{-7}	0.00 015	$\leqslant 0.2$	$\leqslant 0.005$
$^3D_3-{}^3D_2$	0.022	0.065	2.1 ± 0.4	0.40 ± 0.24
$^3D_2-{}^3D_1$	0.20	0.52	2.8 ± 0.5	0.27 ± 0.16
$^3D_3-{}^3D_1$	0.0002	0.00 062	$\leqslant 0.6$	

[a]Reference [13], $T=880$ K.
[b]Reference [26], $T=1100$ K.

cross sections for singlet-triplet transfer of Vadla *et al.* [14,15], which agree with each other fairly well, we expect the values of Brust and Gallagher for $5\ ^3D_J$ fine-structure transfer in Ba-He collisions to be more reliable. In this case, however, the theoretical result for both fine-structure transfer processes strongly deviates from the experimental data. A possible explanation for the observed discrepancies in the case of the ^3D_J fine-structure transfer is that these transfer processes are dominated by couplings at interatomic distances around $5a_0$, where there are significant discrepancies between our potential curves [20] and curves calculated by Czuchaj *et al.* Therefore, it would be desirable to perform close-coupling calculations using the potential curves of Czuchaj *et al.* and to test other e^--He pseudopotentials in our approach.

Fairly good agreement, within a factor of 5, is found between our theoretical result for the process $6\ ^3P_2$-6^3P_1 and the value measured by Kallenbach and Kock at a temperature of $T=1100$ K. We expect this experimental value to be better than the ones for ^3D_J fine-structure transfer since the $6\ ^3P_2$-$6\ ^3P_1$ transfer directly follows the $6\ ^1P_1$-$6\ ^3P_2$ quenching process of the pumped resonance state while the population of the ^3D_J states proceeds through different collisional and radiative channels which might have complicated the data reduction in a fit.

Also given in Tables I and II are the upper limits of the cross sections for the reactions $5\ ^1D_2$-$5\ ^3D_2$, $6\ ^3P_1$-$6\ ^3P_0$, and $5\ ^3D_3$-$5\ ^3D_1$, which are suggested by experimental data. In all cases we find theoretical cross sections consitent with those measurements.

VI. CONCLUSION

We have performed a fully quantum-mechanical close-coupling calculation of singlet-triplet and fine-structure transfer cross sections for colllisions between excited barium and ground-state helium atoms. With the exception of the cross section for ^3D_J fine-structure transfer we find generally good agreement between our theoretical results and the experimental cross sections reported in the literature. A possible explanation for discrepancies in the case of the ^3D_J fine-structure transfer cross sections might be the systematic disagreement between our potential curves and those of other calculations at small interatomic distances. Further experimental and theoretical investigations of these processes are desirable to clarify the remaining discrepancies.

ACKNOWLEDGMENTS

J.B. is indebted to the JILA theory group members for their warm hospitality and their continuous support. J.B. thanks the German Academic Exchange Service for providing financial support from the program HSPII/AUFE. This work was supported in part by the National Science Foundation.

[1] A. R. Malvern, J. Phys. B **11**, 831 (1978).
[2] B. Pouilly, T. Orlikowski, and M. H. Alexander, J. Phys. B **18**, 1953 (1985).
[3] B. Pouilly and M. H. Alexander, J. Chem. Phys. **86**, 4790 (1987).
[4] M. H. Alexander, T. Orlikowski, and John E. Straub, Phys. Rev. A **28**, 73 (1983).
[5] A. L. Zagrebin and S. I. Tserkovnyi, Opt. Spectrosc. **75**, 161 (1993).
[6] A. P. Hickman, J. J. Portman, S. Krebs, and W. Meyer, Phys. Rev. Lett. **72**, 1814 (1994).
[7] M. Harris, J. F. Kelly, and A. Gallagher, Phys. Rev. A **36**, 1512 (1987).
[8] J. Kelly, M. Harris, and A. Gallagher, Phys. Rev. A **37**, 2354 (1988).
[9] W. H. Breckenridge and C. N. Merrow, J. Chem. Phys. **88**, 2329 (1988).
[10] J. P. Visticot, J. Berlande, J. Cuvellier, J. M. Mestdagh, P. Meynadier, P. de Pujo, O. Sublemontier, A. J. Bell, and J. G. Frey, J. Chem. Phys. **93**, 5354 (1990).
[11] J. P. Visticot, P. de Pujo, O. Sublemontier, A. J. Bell, J. Berlande, J. Cuvellier, T. Gustavsson, A. Lallement, J. M. Mestdagh, P. Meynadier, and A. G. Suits, Phys. Rev. A **45**, 6371 (1992).
[12] E. Ehrlacher and J. Huennekens, Phys. Rev. A **50**, 4786 (1994).

[13] J. Brust and A. C. Gallagher, Phys. Rev. A **52**, 2120 (1995).
[14] C. Vadla, K. Niemax, V. Horvatic, and R. Beuc, Z. Phys. D **34**, 171 (1995).
[15] C. Vadla and V. Horvatic, Z. Fiz. A 4, 463 (1995).
[16] E. Czuchaj, F. Rebentrost, H. Stoll, and H. Preuss, Chem. Phys. **177**, 107 (1993).
[17] E. Czuchaj, F. Rebentrost, H. Stoll, and H. Preuss, Chem. Phys. **196**, 37 (1995).
[18] H. Harima, K. Tachibana, and Y. Urano, J. Phys. B **15**, 3670 (1982).
[19] J. A. Neuman, A. C. Gallagher, and J. Cooper, Phys. Rev. A **50**, 1292 (1994).
[20] J. Brust and C. H. Greene, preceding paper, Phys. Rev. A **56**, 2005 (1997).
[21] F. H. Mies, Phys. Rev. A **7**, 942 (1973).
[22] E. E. Nikitin and S. Y. Umanski, *Theory of Slow Atomic Collisions* (Springer, Berlin, 1984).
[23] R. N. Zare, *Angular Momentum* (John Wiley & Sons, New York, 1988).
[24] B. R. Johnson, J. Comput. Phys. **13**, 445 (1973).
[25] F. Mrugala and D. Secrest, J. Chem. Phys. **78**, 5954 (1983).
[26] A. Kallenbach and M. Kock, J. Phys. B **22**, 1705 (1989).